JOURNAL OF CATALYSIS 52, 239–260 (1978)

Modeling Chemisorption Kinetics: Carbon Monoxide on Polycrystalline Platinum

R. G. DONNELLY, M. MODELL, AND R. F. BADDOUR

Department of Chemical Engineering, Massachusetts Institute of Technology, Cambridge, Massachusetts 02139

Received March 30, 1977; revised September 28, 1977

The overall rate of chemisorption of CO on polycrystalline platinum, as determined in temperature-programmed desorption (TPD) experiments, could not be modeled using simple rate laws, but rather was modeled as the sum of the rates of formation of the several distinct species noted in TPD spectra. The rate of formation of each species was determined by deconvoluting TPD spectra corresponding to varying adsorption exposure times, and was modeled using a variant of the Hinshelwood rate law which allowed for site creation. By curve-fitting the experimental rate, an overall model for the chemisorption was proposed. The results are interpreted to indicate that the adsorbed molecules are sufficiently mobile during desorption heating to fill ordered states of minimum energy, and that the chemisorption into these states is noncompetitive and determined solely by the nature of surface. The surface order and species population ratios deduced from the kinetics are in good agreement with surface order and populations deduced in prior low-energy electron diffraction (LEED) studies of the CO Pt system.

1. INTRODUCTION

Potentially rate-limiting processes in heterogeneous catalysis include chemisorption, desorption, surface diffusion, and surface transformation for each of possibly several coexisting discrete adsorbed species. We report here on a first study of the chemisorption dynamics in a well-known system, carbon monoxide on polycrystalline platinum. We have attempted to identify the discrete species chemisorbing, and the surface populations, rates of formation, and mode of surface bonding for each of these species. This has resulted in a mechanistic model for the chemisorption of carbon monoxide on platinum which, though certainly not unequivocal, correctly describes the data recorded here and is consistent with arrangements and densities of adspecies determined in prior work.

An understanding of chemisorption on Pt is of interest because of the wide use of Pt as an industrial catalyst. Pt is a good choice for fundamental studies because of the high purity (99.999 + %) in which it is available and because it can be cleaned to the near-atomically clean state by *in situ* thermal and chemical means (*1–10*). Furthermore, the Pt substrate has been studied in recent years by a variety of techniques, including low-energy electron diffraction (LEED) (*2–15*), Auger electron spectroscopy (AES) (*3–7, 11, 16–19*), field emission microscopy (FEM) (*1, 20*), and molecular beam reflection (*6, 9, 10*). As a result, Pt is a relatively well-characterized material as

0021-9517/78/0522-0239$02.00/0

to surface geometry and cleaniness in the "atomically clean" state.

Carbon monoxide is diatomic and nondissociating, promising simpler chemisorption behavior (and easier modeling) than more complex adsorbate molecules. The chemisorption of CO on Pt is known to be simpler than that of CO on many other transition metals. For example, there is quite general agreement that the CO–Pt bond is linear through the carbon atom, as deduced from infrared (*21–27*) and other (*4, 5*) studies, as opposed to the bridged or lying-down mode invoked in addition to the linear mode for other CO–metal adsorptions (*28*).

Several studies of the CO–Pt system have been accomplished recently. The structure and energetics of the CO adlayer on Pt have been inferred in LEED studies (*4, 5, 11, 14, 29–31, 49*), in reflection–absorption infrared spectroscopy (*27*), and in a recent uv photoemission study (*19*). Regimes of surface mobility of CO over various single crystal faces of Pt have been determined in FEM work (*20*). A few studies reporting on chemisorption dynamics within the CO–Pt system have appeared, although for the most part overall adsorption (as opposed to discrete species adsorption) and desorption kinetics have been investigated (*16, 27, 32–36*), with reports of high initial sticking coefficients (*27, 33–35, 49*), approximate first-order pressure dependence of adsorption rates (*34, 35*), and first-order population dependence of desorption rate (*34*). Finally, temperature-programmed desorption has been utilized to varying extent in a number of studies (*13, 14, 19, 27, 36–38, 49*).

2. METHODS

The temperature-programmed desorption (TPD) technique is potentially capable of generating data on many aspects of chemisorption dynamics. There are a number of problems that have limited the usefulness of TPD in studies in catalysis, however. We have attempted in the work we report here to avoid these shortcomings wherever possible by modification of experimental procedure and analytical methods which we have described elsewhere (*39*).

Briefly, the technique applied here was as follows. The substrate sample was heated to high temperature to remove adsorbed species, and was cooled only after achieving the ultrahigh vacuum level background pressures [9×10^{-11} Torr, (1 Torr = 133.3 nm^{-2})], in order to maintain substrate cleanliness. The substrate was then exposed to a step of the adsorbate gas at pressure P_a for the adsorption exposure time t_a.

The material balance on the gas phase within the TPD chamber could be solved to yield the instantaneous total rate of desorption from the substrate at all times during the desorption heating period (*39*). The locus of instantaneous total rate of desorption versus substrate temperature is then termed the *desorption spectrum*. We mention in passing that the solution for the desorption spectrum was possible only after quantifying the interaction of the gas phase with the so-called "wall phase" under the transient conditions during a desorption. Independent experimentation was required to model this phenomenon, as we discuss elsewhere (*40*).

The desorption spectrum is viewed as the composite of the desorption spectra of the several discrete adspecies, i, and thus deconvolution of the composite spectrum yields the desorption spectra for the various adspecies. These single-species spectra are interpreted in a model for single-species desorption in order to relate the instantaneous desorption rate, r_{d_i}, to the desorption activation energy, E_{d_i}, the desorption preexponential, ν_i, the desorption order for species i, and the linear heating rate, β. The Polanyi–Wigner model for desorption was

assumed,

$$r_{d_i} = -\frac{dn_i}{dt} = \nu_i n_i e^{-E_{d_i}/RT}, \qquad (1)$$

in which n_i = surface population of adsorbed species i and in which the parameters are assumed constant. (Although, in general, species may desorb according to either first- or second-order kinetics, we found that first-order desorption kinetics accurately modeled the carbon monoxide desorption from polycrystalline Pt.) The relationships among desorption peak position and shape and the energetic and kinetic parameters are fully documented elsewhere (*39, 41–43*) and will not be developed here.

The populations, n_i, within the various adstates i are then determined as the integral of Eq. (1), solved for the parameters determined in deconvolution. By determining the various n_i for experiments in which adsorption exposure duration, t_a, is varied at a single adsorption pressure, P_a, and differentiating the n_i data with respect to t_a, rates of population of these individual adstates can be obtained.

The apparatus in which these experiments were performed and procedural details are discussed elsewhere (*39*). The substrate sample was a 5 *N* pure polycrystalline Pt filament of 0.0051-cm diameter and 30-cm length. Research-grade carbon monoxide and pretreatment gases were used.

3. RESULTS

Deconvolution of Desorption Spectra

In Fig. 1 is shown a family of desorption spectra corresponding to adsorption for varying durations at the CO adsorption pressure 1×10^{-8} Torr. The number of peaks required to deconvolute the desorption spectra and the location of each on the temperature axis (i.e., the E_d value of each) were determined in a parametric optimization routine in which values of E_{d_i}, ν_i, and the surface population for i, n_i, were varied independently. The deconvolution attempts began with the lowest coverage spectrum

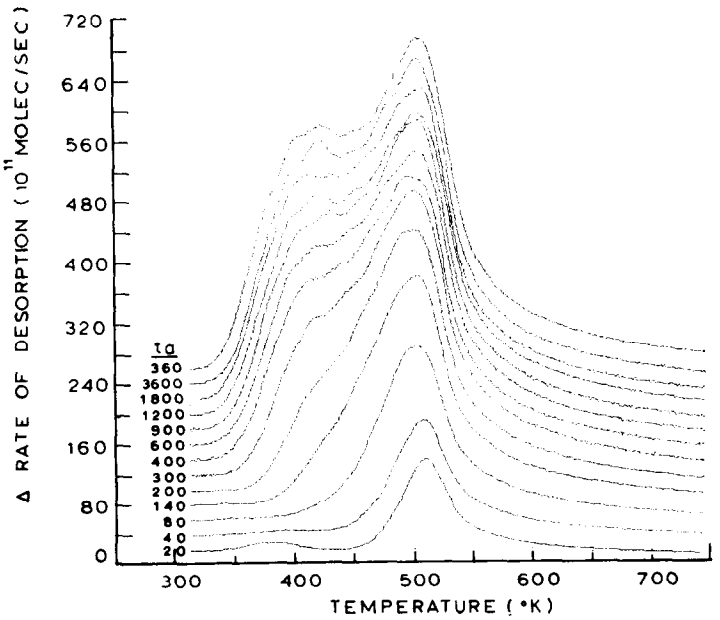

FIG. 1. Family of TPD spectra; adsorption exposure 20 to 3600 sec at 1×10^{-8} Torr and 360 sec at 1×10^{-7} Torr at 23°C; β = 15.6°K/sec (*39*).

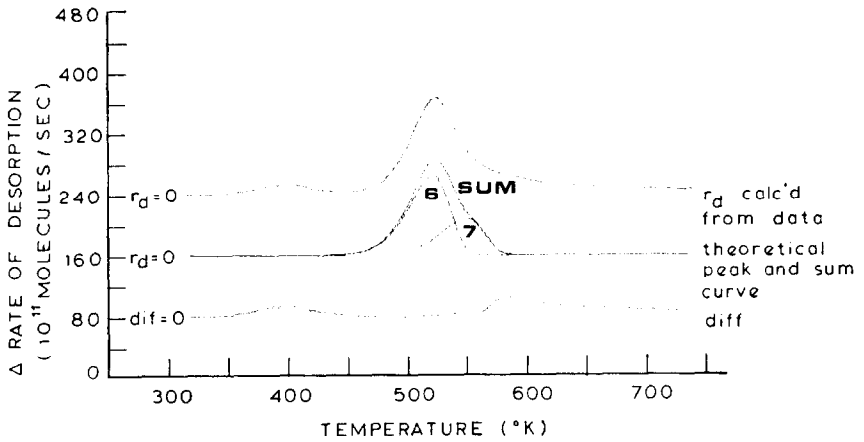

FIG. 2. Deconvolution of TPD spectrum corresponding to adsorption exposure of 20 sec at 1×10^{-8} Torr at 23°C; $\beta = 15.6$°K/sec.

(corresponding to 4% of monolayer coverage) and continued sequentially with higher coverage spectra, adding new species peaks and moving and/or increasing in height established species peaks as necessary to obtain best fit with the fewest possible species.

The lowest-coverage case, that for adsorption for 20 sec at 1×10^{-8} Torr (run 37), is illustrated in Fig. 2 along with the proposed deconvolution for this spectrum. The two theoretical peaks, the sum of the peaks, and the difference between the desorption spectrum and the sum are shown. The low-temperature edge was found to be fit essentially perfectly with the theoretical single-species desorption peak of $E_d = 30.8$ kcal/mol (1 kcal/mol = 4186.8 J/mol) (to be later identified as species 6). The high-temperature edge of the spectrum showed gradual decay, necessitating the introduction of a higher-energy second species at $T_p = 554$°K and $E_d = 32.6$ kcal/mol (to be later identified as species 7). The remainder of the tail to the high-energy side was not deconvoluted. The tail portion of the spectrum typically amounted to 15% of the total surface population and can be attributed to temperature maldistribution in the substrate or adsorption at defects and other high-energy sites. It is noteworthy that the adjacent adstate on the low-energy side of the major peak (to be later identified as species 5) is not populated at this low coverage. (The broad, low peak centered about 425°K was found to be caused by the desorption of, or the reaction to form mass 44. This peak formed reproducibly after subsequent 20-sec exposures, but was not seen at longer exposures. Thus, potential carbon laydown was limited and apparently reversible.)

As coverage increased after longer adsorption exposure times, adstates were found to be populated approximately consecutively in the direction of lower energy. For the high-coverage ($t_a = 1200$ sec) run the deconvolution procedure resulted in the seven species illustrated in Fig. 3. The smoothed shape of the desorption spectrum and the sum curve can be seen to match well. It is noteworthy, in addition, that the desorption spectrum fine structure is itself reproduced approximately in the sum curve.

The most obvious question concerning the uniqueness of this deconvolution with seven species is whether it can be accomplished with fewer species. We found that deconvolution with only one less peak resulted in significantly poorer fit of the desorption spectrum (*39*). A second ques-

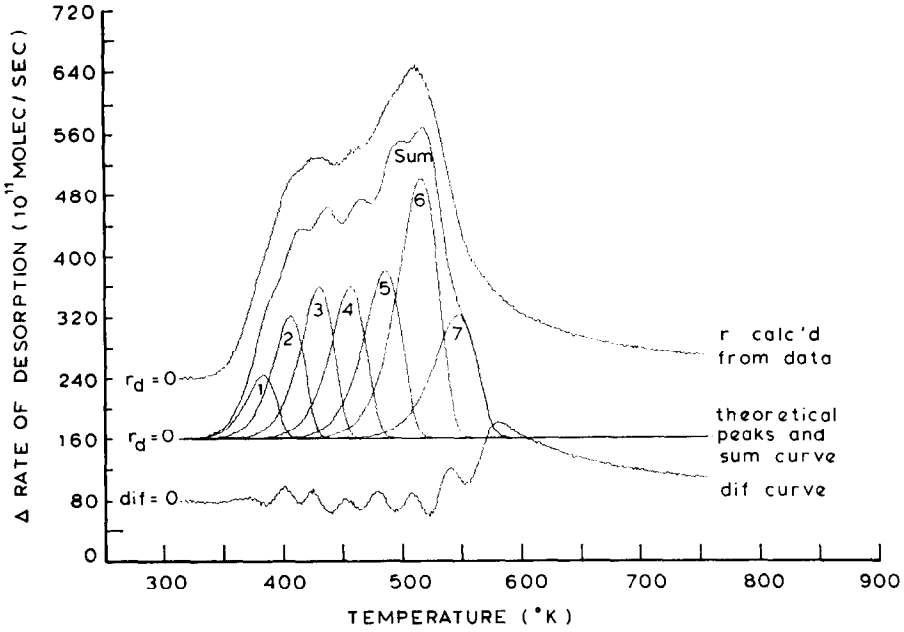

FIG. 3. Deconvolution of TPD spectrum corresponding to adsorption exposure of 1200 sec at 1×10^{-8} Torr at 23°C; β = 15.6°K/sec (*39*).

tion about the uniqueness of the proposed deconvolution concerns the confidence with which peak position (species E_d) and peak height (species population) can be specified for each of the seven species identified. We found that movement of a peak as few as 2 to 3°K along the temperature axis caused notable deterioration of fit (*39*).

We contend on this basis that the chemisorption of carbon monoxide on polycrystalline Pt can be adequately characterized by the existence of seven distinct desorption surface states, which are populated to differing extents as coverage (adsorption time) increases. These adstates are summarized in Table 1, numbered in order of their increasing activation energies to desorption. With one exception (peak 6 to a small extent at low coverage only), adstates were found to be characterized by fixed E_d over the entire coverage range of their existence (from 4 to 100% of monolayer coverage).

TABLE 1

The Seven Desorption Surface States for CO on Polycrystalline Platinum

Species number	E_d[a] (kcal/mol)	T_p[b] (°K)
1	22.5	381
2	23.9	404
3	25.3	427
4	27.0	455
5	28.8	483
6	30.6	514
7	32.6	545

[a] For $\nu = 10^{13}$ sec^{-1}.
[b] β = 15.6°K/sec.

Kinetics

The *overall* surface population is determined by integrating the desorption spectrum over the entire desorption time. Overall surface population is given as a function of adsorption exposure time in Fig. 4. (The nonzero value at $t_a = 0$ corresponds to adsorption at the background pressure during the substrate cooling period.) The instantaneous rate of the

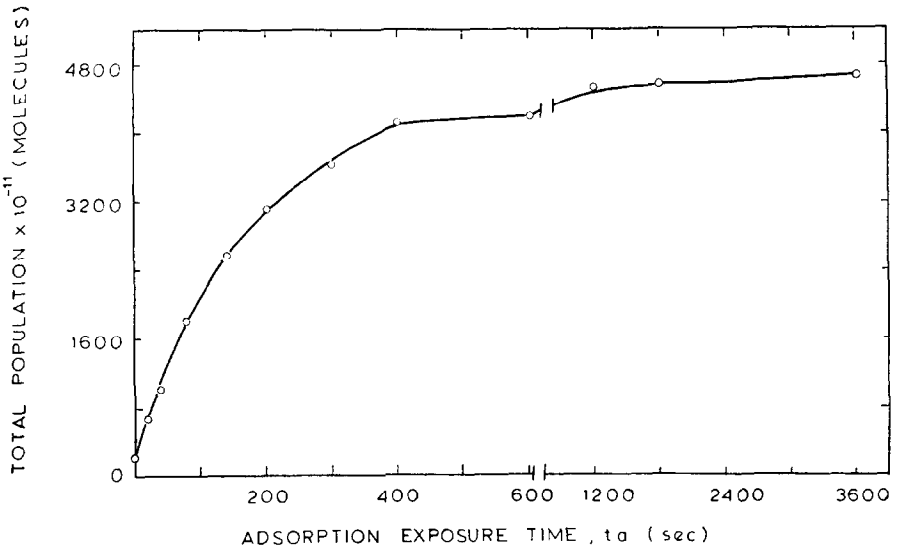

FIG. 4. Total population vs adsorption exposure time at 1×10^{-8} Torr at 23°C. (Note abscissa scale change.)

overall chemisorption was determined by differentiating the data in Fig. 4, with respect to adsorption exposure time, with the results shown in Fig. 5. As is apparent from the complexity of the curve in Fig. 5, the overall adsorption kinetics cannot be modeled according to the well-known simple theories: that of Hinshelwood, as a function of the fraction of available sites,

$$r_a = k(1 - \theta), \tag{2}$$

or that of Elovich, as a function of changing activation energy to adsorption,

$$r_a = ae^{-b\theta}, \tag{3}$$

where k, a, and b are empirically determined

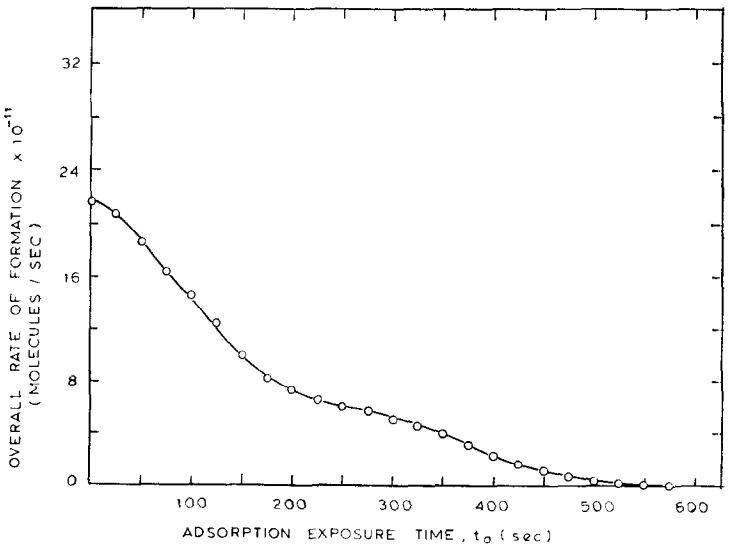

FIG. 5. Overall rate of chemisorption vs adsorption exposure time at 1×10^{-8} Torr at 23°C.

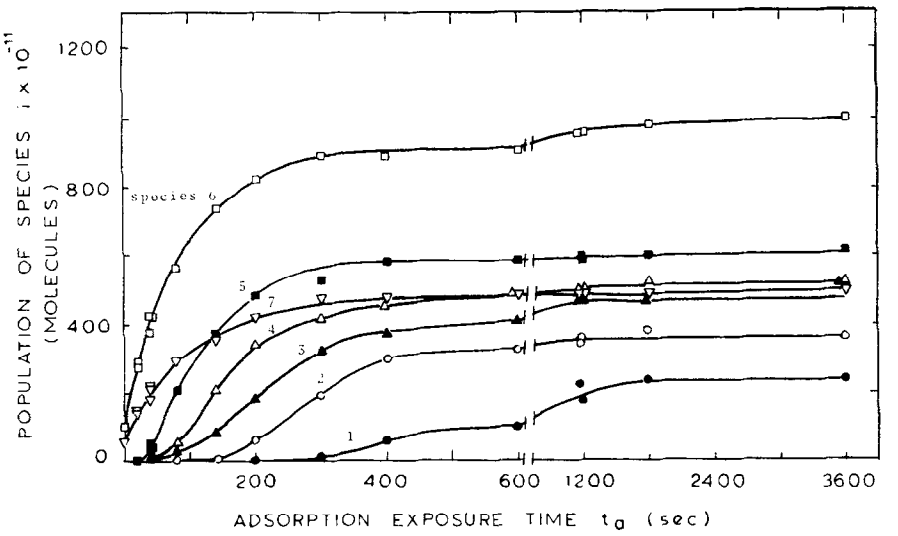

FIG. 6. Populations of individual species vs adsorption exposure time at 1×10^{-8} Torr at 23°C. (Note abscissa scale change.)

constants. Thus, we examine the kinetics of chemisorption into the discrete adstates, which in sum would then give overall adsorption kinetics.

We define the rate of formation, r_{f_j}, of the *single species* j as

$$r_{f_j} = \frac{dn_j}{dt_a}, \tag{4}$$

where n_j is the population within adstate j

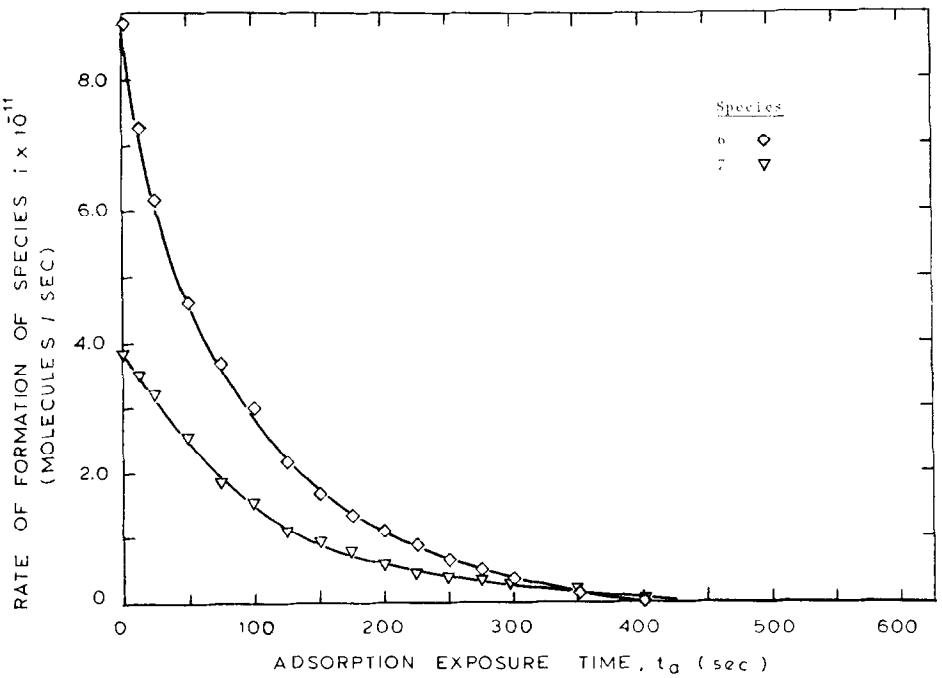

FIG. 7. Rates of formation of species 6 and 7.

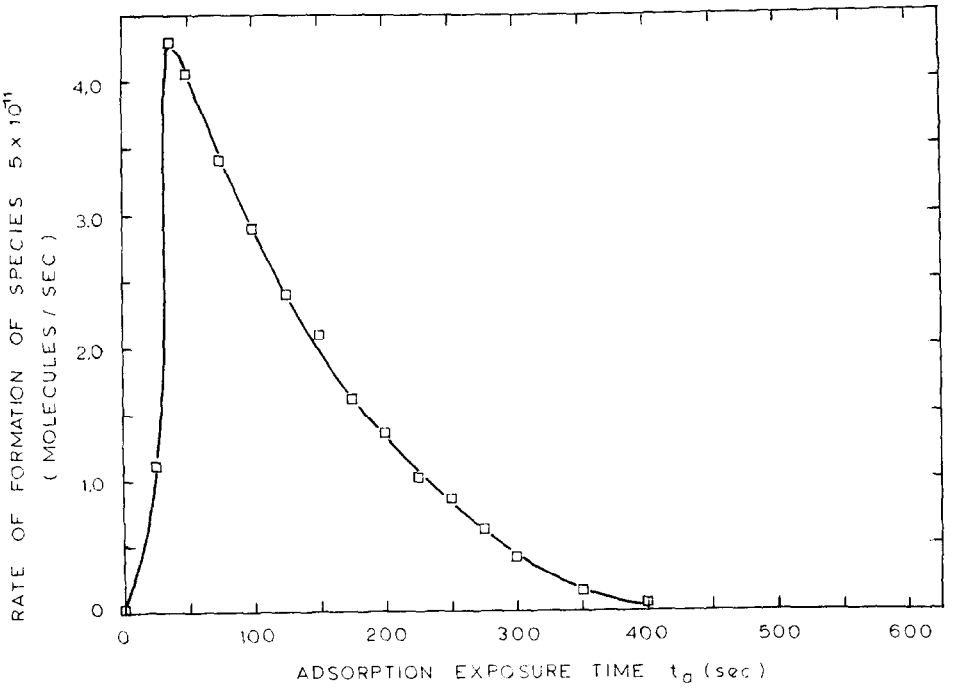

FIG. 8. Rate of formation of species 5.

as determined from deconvolution of TPD spectra, and where the choice of t_a in the denominator allows comparison of relative formation rates for all species. We must stress that the rate of formation of j *as determined from TPD spectra* is not neces-

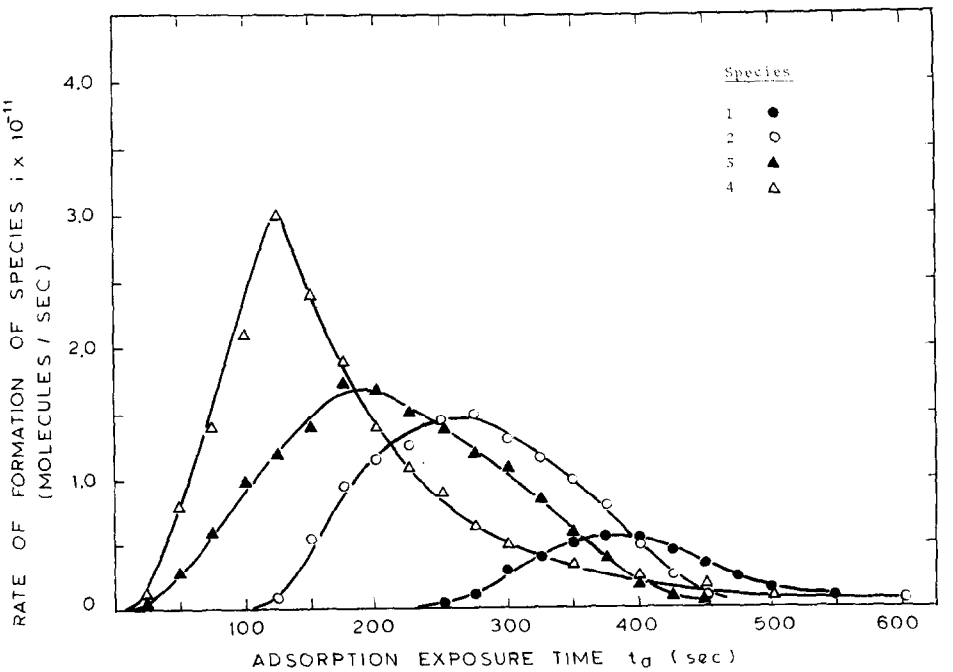

FIG. 9. Rates of formation of species 1, 2, 3, and 4.

sarily equivalent to the rate of chemisorption into state j, r_{a_j}, since transformation between the state into which chemisorption occurs and the state from which desorption occurs cannot necessarily be excluded.

The kinetics of formation of the various single species for CO on Pt are determined after deconvoluting the family of desorption spectra illustrated in Fig. 1. This procedure yields populations in the adstates as a function of adsorption exposure time, data which are given in Fig. 6. An indication of the accuracy of these measurements ($\sim 2\%$ of saturation population) is seen in the reproducibility illustrated for several of the data points. The instantaneous rates of formation of the individual species are then determined by differentiating the population curves in Fig. 6 according to Eq. (4). The rates of formation of species 6 and 7 are given in Fig. 7, of species 5 in Fig. 8, and of species 1 through 4 in Fig. 9.

4. DISCUSSION

Modeling the Chemisorption

From Figs. 7, 8, and 9 it is seen that only species 6 and 7, the most strongly bound species, apparently form with nonzero rates from the first moment of exposure, whereas the more weakly bound species begin to form only after longer adsorption exposure. This behavior is explained in either of two ways:

(i) Each of the adstates found in a high-coverage desorption spectrum corresponds to a different type of site on the surface—different lattice planes, dislocations, plane edges, etc. Chemisorption into each of these states occurs directly after even short adsorption exposure, the various states being filled according to sticking probability statistics. During desorption heating, however, the more weakly bound species transform (diffuse) to fill and subsequently desorb from the stronger states.

(ii) The various energetic states seen in the desorption spectrum arise *both* from different types of sites on the various exposed lattice planes *and* from different hybridization of the bonds on any one exposed lattice plane. Different bonding hydridization could be required, for example, if a surface site became surrounded by nearest-neighbor adsorbed species. None of the more weakly bound chemisorbed species form at short exposure, then, since the weaker energetic states cannot exist until an appreciable adsorbate population in the stronger states is present.

Both kinds of behavior are plausible, and neither can be discarded a priori. We believe that the weight of evidence argues for the latter as against the former possibility, however.

There is considerable evidence (*5, 16, 35, 44–46*) that well-annealed high-purity Pt exists predominantly as large single crystal-like lattice planes of low index. Then if the former explanation applied, the transformation of more weakly bound adsorbed species into more strongly bound species during the course of the TPD would require long-range diffusion across these large surface planes, a relatively slow process. At the moderate heating rates utilized in our work, such long-range diffusion would be detected at short adsorption times by the presence of at least small amounts of weaker species which desorbed before they were able to transform. The absence of such species at short adsorption times is unequivocal. Thus, the second explanation for the absence of the more weakly bound species at the initial adsorption exposure appears to be the more likely. This is a postulate which can be tested by curve-fitting the rate of formation data for individual species with theoretical models which require the appropriate nearest-neighbor sites to be filled. We now construct such a model.

A general model of the chemisorption must, according to the view espoused in

(ii) above, allow certain energetic states characteristic of the initially bare surface to be filled with maximum rate initially and to subsequently become saturated, and must allow certain other energetic states to be created as surface population increases, themselves to subsequently become saturated. A modified Hinshelwood-type expression would model chemisorption into the type of energetic site filled with maximum rate initially.

$$\frac{dn_j}{dt_a} = k_j(n_f - n)_j{}^p, \tag{5}$$

where k_j = formation rate constant for species j; n_f = total number of sites of type j at saturation; n = number of filled sites of type j; and p = number of adjacent empty sites needed for formation of species j; and where t_a is used in the differentiation so as to fit the r_{f_j} values of Eq. (4). Equation (5) permits energetic state j to become saturated before saturation coverage of the surface occurs. An additional modification of a Hinshelwood-type expression would model chemisorption into the created-type energetic site,

$$\frac{dn_j}{dt_a} = k_j(n)_I{}^{p'}(n_f - n)_J{}^p, \tag{6}$$

where j refers to the species chemisorbed on the created site; I refers to the p' adjacent chemisorbed species $(i + k + \cdots)$ which created the site; J refers to the species $(j + l + \cdots)$ which compete for the p adjacent sites needed for formation of species j; n_f = total number of sites of type J at saturation; and k_j = a formation rate constant. The right-hand side of Eq. (6) is seen to be proportional to the probability that an empty site will be a j-type (created) site. We should note that no gas-phase pressure dependence or precursor-state concentration dependence is included in either of Eqs. (5) or (6). Rate of formation curves successfully fit by these expressions must therefore have constant "driving force" for population of a site (i.e., the pressure dependence is included in the rate constant, k_j).

We treat first the species which formed with maximum rate at $t_a = 0$. A first-order ($p = 1$) rate expression of the form of Eq. (5) successfully fit the instantaneous rates of formation of species 6 and 7 from the point $t_a = 0$ sec, and of species 5 from the point just past the maximum formation rate at $t_a = 40$ sec. This is illustrated for species 5, 6, and 7 in Fig. 10. (The failure of curve B to intersect the origin is attributed to a slight ambiguity in peak assignation due to the tail portion of the spectrum.)

A special note on the attempts to fit species 5 kinetics of formation is in order. Based upon the deconvolution results, species 5 apparently forms at zero rate initially. However, we were unable to treat species 5 as a created energetic state with plausible expressions of the form of Eq. (6). An alternative explanation of the species 5 behavior is that this species represents adsorption on the Pt(100) lattice plane, which for clean surfaces or very low coverage is known to exist as a reconstructed pseudo-(111) plane (*4, 5, 47, 48*). We did note a small shift in apparent species 6 position, which might then be ascribed to the changing contribution to this peak of molecules which reside on and desorb from a pseudo-(111) plane at low coverage, but which for greater coverage reside on and desorb from the true-(100) plane. In this way species 6 was tentatively identified with the true-(111) plane. Finally, species 7 was identified with one of the remaining low-index planes, the (110) or a similar plane.

The species 1 through 4, which form at zero rate initially, can be assumed to require sites to be created before they can form. It is plausible, then, that species 5, 6, and 7 are responsible for the creation of some of

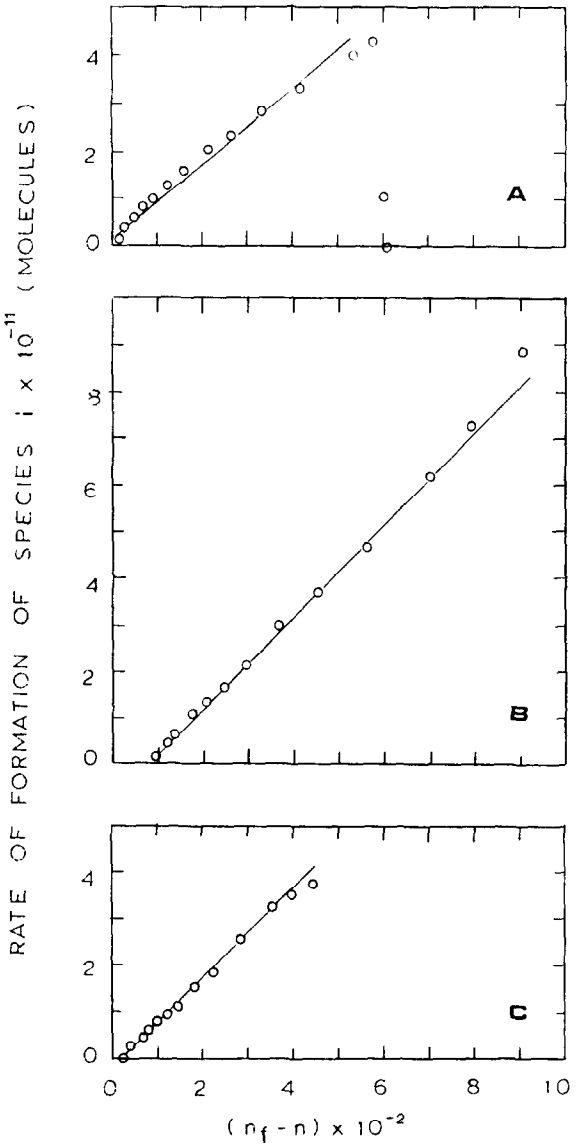

FIG. 10. Test of first-order formation rate: (A) species 5; (B) species 6; (C) species 7.

the sites for species 1 through 4 according to the model of Eq. (6). The more weakly bound species j may be identified as depending upon the presence of the more strongly bound species i (or $I=i+k+\cdots$) for creation of its site by trial and error application of Eq. (6), using experimentally determined populations for the various species i (or $I = i + k + \cdots$) and for the species j of interest, and using reasonable values of p' and p. The trial theoretical curve calculated from Eq. (6) is then scaled to the maximum experimental formation rate value for species j to allow comparison of the curve shapes.

Assuming that species 5, 6, and 7 chemisorbed independently onto different exposed lattice planes, rate of formation curves for species 1 through 4 were fit with appropriate expressions of the form of Eq. (6), using populations of species 5, 6, and 7 to determine site creation probabilities. A typical

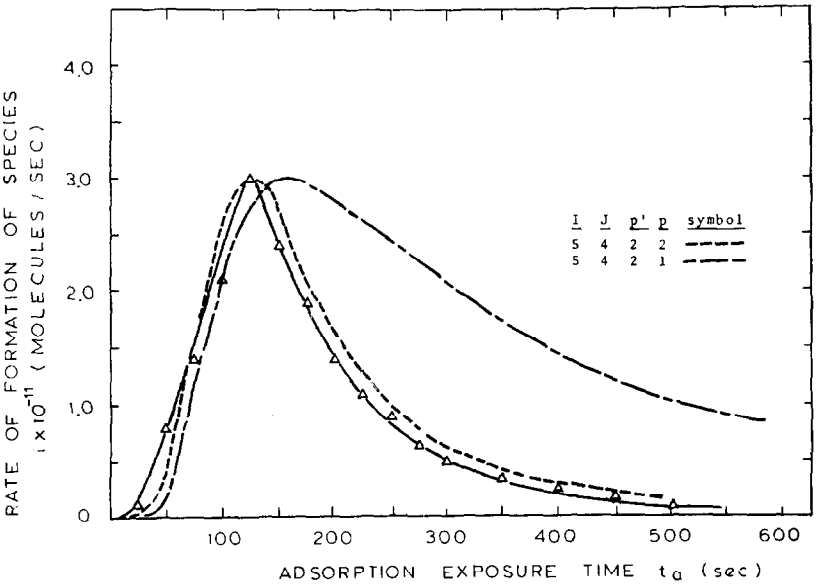

FIG. 11. Curve-fitting the rate of formation for species 4 (best and typical poor fit).

good fit is illustrated in Fig. 11 for species 4 using $I = 5$, $J = 4$, $p' = 2$, $p = 2$ in Eq. (6). A typical poor fit is also given in Fig. 11 for the very similar case $I = 5$, $J = 4$, $p' = 2$, $p = 1$. All formation rates were fit in this manner, resulting in more than a single good fit only in the cases of species 3 and 4. A summary of the success-

TABLE 2

Successful Curve Fits of Experimental Rates of Formation, $\frac{dn_j}{dt_a} = k_j(n)_I{}^{p'}(n_I - n)_J{}^{p}$

Reference	Species j	Site creation		Sites available		Assumed lattice plane	
		I	p'	J	p	(hkl)	z^a
(*a*)	7	—	—	7	1	(110)	~4
(*b*)	6	—	—	6	1	(111)	6
(*c*)	5	(100)-rearrangement		5	1	(100)	4
(*d*)	4	5	2	4	2	(100)	4
(*e*)	4	6	4	4	2	(111)	6
(*f*)	4	7	4	4	2[b]	(110)	~4
(*g*)	3	6	4	3	1	(111)	6
(*h*)	3	7	4	3	1	(110)	~4
(*i*)	2	5 + 4	4	2	1	(100)	4
(*j*)	2	6	6	2	1[c]	(111)	6
(*k*)	1	6 + 3	6	1	1[d]	(111)	6
(*l*)	1	5 + 4	4	1	1[d]	(100)	4
(*m*)	1	7	4	1	1[d]	(110)	~4

[a] $z \geq p' + p - 1$ = indicated coordination.
[b] This possibility excluded on the basis of the indicated coordination exceeding the actual.
[c] Fair fit only.
[d] No successful fits found; these are fair to poor only.

ful curve fits of the experimental rates of formation is given in Table 2.

An interesting feature of the chemisorption which arises from the foregoing formation rate analysis concerns the significance of the sites-available dependence of the formation rate. A significantly better fit of the formation rate curve for any species j resulted when dependence of the formation rate on the sites available *for species j only* was assumed (i.e., when $J = j$). This was the case for the formation rates for all seven species identified. Briefly the significance of such a finding is: (i) that the formation of the various distinct species is noncompetitive, so that the maximum number of the various kinds of sites available is fixed by the nature of the substrate surface; and (ii) that the adsorbed species are sufficiently mobile under the thermally excited conditions of TPD to fill these sites as they are created.

Model Discrimination

Based upon the results listed in Table 2, the plausible models describing the overall chemisorption are now considered. The mechanisms which proved successful in predicting the correct shapes of the rate of formation curves were combined in such a way as to be consistent with:

(i) the assumption based on extensive literature cited above that three low-index lattice planes predominated on the substrate, the (111) with coordination 6, the (100) with coordination 4, and the (110) or similar plane with coordination "approximately" 4;

(ii) the postulate, discussed briefly above, that species 6 resided on the (111) plane, species 5 on the (100) plane, and species 7 on the third plane;

(iii) the assumption that the four less stable species, 1, 2, 3, and 4, also existed on the (111), the (100), and some third lattice planes, the sites for their formation being created by the presence on the plane of one of the more stable species;

(iv) the requirement that some plausible reason for the distinctness of species be evident, on the basis of possible geometric ordering of the various species populations on the lattice planes.

On this last point, we take a moment here to emphasize that the coordination, z, of a surface atom on a particular lattice plane places on the exponent values the restriction $z \geq p' + p - 1$, since at saturation each set of p j-type sites which is filled must have adjacent to it a set of p' i-type sites which is filled. This fixes at least one limit for the ratio between saturation populations of i and j. For example, on a lattice plane with coordination number 4, with $p' = 4$ = no. of filled i-type adjacent sites required to form a j-type site, and $p = 1$ = no. of adjacent empty sites required for formation of species j, the ratio $(n_i/n_j)_{\text{sat}} \geq 1$. The ratio would exceed unity if a filled i-type site had adjacent filled i-type sites.

In Table 3 are listed three plausible models for the overall chemisorption, representing different assignments of the various species to the three lattice planes via the mechanisms listed in Table 2. On the basis of item (iv) above, suggested ideal population ratios at saturation for each species on a particular plane are given, along with the resulting ideal fractional coverage at saturation. Actual population ratios at saturation are given for comparison. In addition, the number of chemisorption sites for each plane is given, along with the total number of sites and total surface area based thereon. The numbers of sites are calculated from ideal planar fractional coverages and experimental planar populations, as indicated in the notes to Table 3.

A criterion of some utility in discriminating among the plausible models was the predicted initial sticking probabilities, s_0, for the overall chemisorption. The s_0 values

TABLE 3

Summary of Plausible Chemisorption Models

	Model	Plane	Chemisorption to saturation population ratios		θ_{ideal}	Sites for chemisorption		Apparent sticking probabilities[c]		Successful curve-fit mechanisms[d]
			Ideal	Actual		Planar[a] ($\times 10^{-11}$)	Total[b] ($\times 10^{-11}$)	Initial	Maximum per available site	
I	7-␣[e]	(110)	(1:1)	(1:1)	0.50	1000		1.82[f]	1.86[f]	(a)
	6-3-1	(111)	(2:1:1)	(2:0.96:0.48)	1.00	2000		1.70[f]	1.79[f]	(b) (g) (k)
	5-4-2-␣	(100)	(4:3:2:3)	(4:3.5:2.5:3)	0.75	2000		—	1.23	(c) (d) (i)
						5000	5940 (0.413 cm²)[g]	1.34		
II	7-1-␣	(110)	(2:1:1)	(2:0.96:1)	0.75	1000		1.82[f]	1.86[f]	(a) (m)
	6-3-␣	(111)	(2:1:1)	(2:0.96:1)	0.75	2000		1.70[f]	1.79[f]	(b) (g)
	5-4-2-␣	(100)	(4:3:2:3)	(4:3.5:2.5:3)	0.75	2000		—	1.23	(c) (d) (i)
						5000	5940 (0.413 cm²)[g]	1.34		
III	7-3	(110)	(1:1)	(1:0.97)	1.00	1000		1.82[f]	2.87	(a) (h)
	6-2	(111)	(3:1)	(3:1.1)	1.00	1330		2.56[f]	2.76	(b) (j)
	5-4-1-␣	(100)	(4:5:3)	(4:5.0:3)	0.75	1830		—	1.35	(c) (d) (l)
						4160	5100 (0.356 cm²)[g]	1.55		

[a] Number of sites ratioed up based on θ_{ideal} and the saturation population on the plane, and assuming one site per molecule.

[b] Total number of sites = sum of the sites on the three planes, plus one site per molecule for each "tail-species" molecule.

[c] Based on Eq. (7) with $z = 3.9 \times 10^{20}$ for CO at 25°C.

[d] See Table 2.

[e] Nomenclature: ␣ refers to surface sites unfilled at saturation.

[f] Initial sticking probability calculated for species 6 (and to a lesser extent for species 7) is high because of the contribution of species 5 initially (see text).

[g] Total adsorption area based on the various planar and tail sites and the site densities, ρ_s: $\rho_{s(111)} = 1.50$; $\rho_{s(100)} = \rho_{s\,tail} = 1.30$; $\rho_{s(110)} = 1.84$ (as defined for adsorption in the "valleys"); (units = sites per square centimeter $\times 10^{-15}$). By comparison, geometric area of filament is 0.485 cm².

are based on the numbers of the various planar kinds of sites, as illustrated in Table 3, and on the theoretical site densities for the (111), (100), and (110) planes. As shown in Table 3, $s_{0_{overall}} = 1.34$, 1.34, and 1.55 for Models I, II, and III, respectively, based on the areas for chemisorption calculated from the total sites available. (Based on the geometric surface area of the filament, $s_{0_{overall}} = 1.14$.) Errors in pumping speed and absolute pressure determinations could account for $s_{0_{overall}}$ ranging from approximately 0.6 to 1.4. Then on this basis Models I and II are slightly favored over Model III.

Further discrimination among the various models can be accomplished via the calculation of the sticking probability per available site, s, throughout the course of the chemisorption. This is defined for each lattice plane as

$$s_{(hkl)} \equiv \frac{r_{a_{hkl}}(t_a)}{ZP_a[n_f - n(t_a)]_{(hkl)}/\rho_{s(hkl)}}, \quad (7)$$

where (hkl) refers to the particular lattice plane; $r_{a_{hkl}}(t_a)$ = rate of adsorption on the lattice plane at time t_a (molecules/sec), according to the particular model; Z = impingement rate (molecules/sec-cm^2-Torr); P = gas-phase adsorption pressure (Torr); $[n_f - n(t_a)]_{(hkl)}$ = number of nonfilled sites in the lattice plane (cm^{-2}), according to the particular model (i.e., the difference between the total sites assumed on the plane and the sum of the populations of all species on the plane). One adsorbed molecule is assumed to fill one site.

These calculated sticking probabilities per available site, s, are plotted for the various models in Fig. 12 for the (110) lattice plane and in Fig. 13 for the (111) lattice plane. Then a model which leads to the calculated $s_{(hkl)}$ exceeding unity by greater than the experimental error would be held in disfavor. A second discerning feature is the course of the $s_{(hkl)}$ curve as a function of planar population. For ideal chemisorption of a single species in the Hinshelwood picture (i.e., no adsorbate–adsorbate interactions, no change in E_a or E_d with coverage, etc.), $s_{(hkl)}$ would be expected to equal unity throughout the course of the adsorption. Nonideal effects (ad-

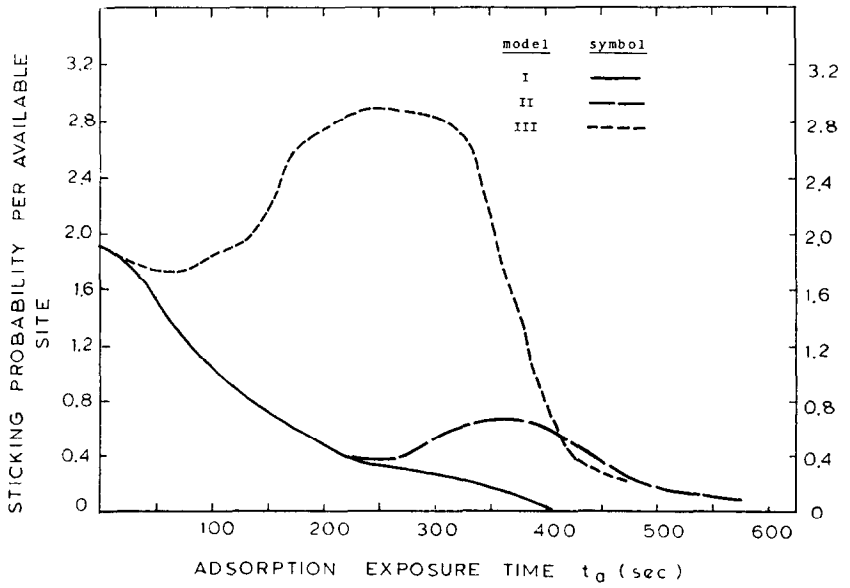

FIG. 12. Sticking probability per available site on the postulated (110) plane.

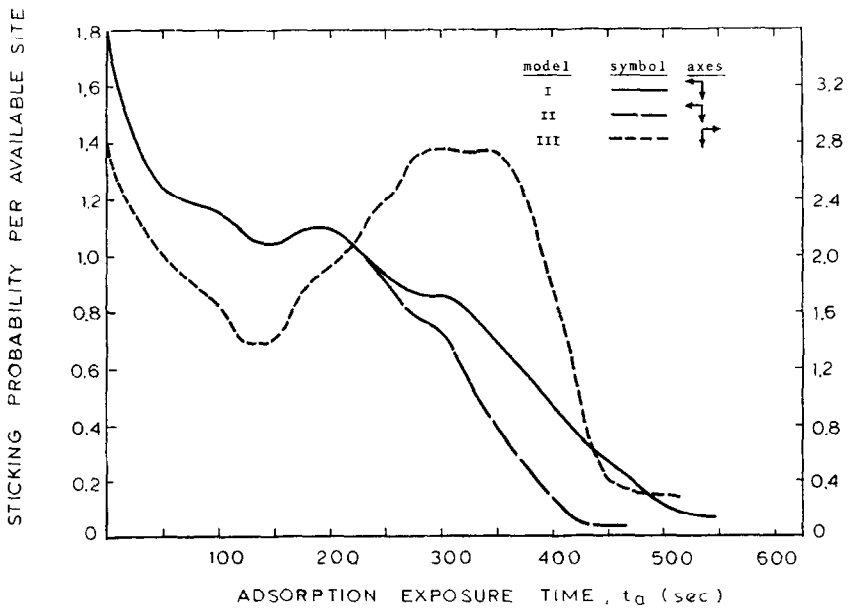

FIG. 13. Sticking probability per available site on the postulated (111) plane.

sorbate–adsorbate interactions) should increase in importance monotonically with increasing population. Hence, reasonable models for the chemisorption on a particular plane would be expected to result in an approximately monotonic decrease of $s_{(hkl)}$, if any; any increase would be at most small and would coincide with the completion of a particular phase.

The calculated sticking probabilities per available site presented in Figs. 12 and 13 argue against Model III on the basis of both the shape of the curves and the high values. Figure 12 indicates that $s_{(110)}$ exhibits both a minimum and a maximum, with an initial value of approximately 1.9 and a value at the maximum of approximately 2.9. Similar behavior is seen in

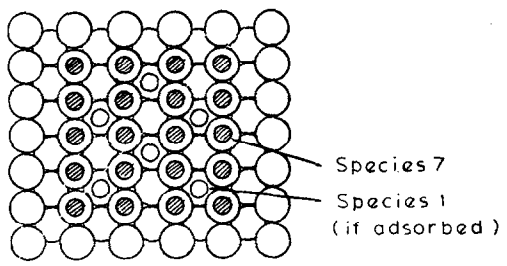

FIG. 14. Structure of the adsorbate for the (110) plane, species 7 (and 1).

TABLE 4

Constant-Pressure Rate of Formation Expressions for the Individual Species[a]

Expression	Postulated lattice plane
$r_7 = k_7(n_f - n)_7 P_{CO}$	(110)
$r_6 = k_6(n_f - n)_6 P_{CO}$	(111)
r_5[b] $= k_5(n_f - n)_5 P_{CO}$	(100)
$r_4 = k_4(n_5)^2(n_f - n)_4{}^2 P_{CO}$	(100)
$r_3 = k_3(n_6)^4(n_f - n)_3 P_{CO}$	(111)
$r_2 = k_2(n_5 + n_4)^4(n_f - n)_2 P_{CO}$	(100)
$r_1 = k_1(n_6 + n_3)^6(n_f - n)_1 P_{CO}$	(111)
or	or
$= k_1'(n_7)^4(n_f - n)_1 P_{CO}$	(110)

[a] The dependence on the first order of pressure is approximately correct, based on equivalent-exposure results over narrow ranges of pressure.

[b] Species 5 forms at zero rate initially, because the Pt-(100) substrate resides in a pseudo-(111) arrangement until appreciably covered by adsorbate; this can be expressed here as a value for n_f which changes with time up to approximately 40-sec adsorption exposure at 1×10^{-8} Torr CO.

Fig. 13 for $s_{(111)}$ according to Model III, in which both initial and maximum values are approximately 2.9. [The high *initial* values on these two figures exceed those attributable to experimental error and are believed to be due to the contribution of species 5 initially, i.e., while the (100) plane still exists as a reconstructed pseudo-(111).] The results for the (110) plane in Fig. 12 show that the curve for Model I decreases monotonically, while that for Model II shows a minimum and maximum. The $s_{(111)}$ curves in Fig. 13 show approximate monotonic decreases with adsorption exposure, for both Models I and II. The $s_{(100)}$, values which are not shown here, were found to be reasonable for all models. Strong indications for or against either Model I and II are not found on the basis of these criteria, therefore. However, either of the Models I or II is quite strongly favored in comparison with Model III, and Model I may be slightly favored over Model II.

The rate of formation expressions for the individual species were thus determined to be those listed in Table 4.

Implications

A feature worth some discussion is the distinctness of the adsorbed species before TPD heating begins. We must emphasize that nowhere in the preceding analysis have the individual species on a given lattice plane been required to be distinct *before* desorption heating begins. Thus, the molecules chemisorbed at saturation on the (100) lattice plane, for example, may all reside in identical energetic states at the adsorption temperature. When the substrate temperature is raised, however, desorption occurs from the distinct energetic states 2, 4, and 5, in that order, as determined above. In this case the state from which species 2 (the least stable species) desorbs may closely approximate the energetic state in which all species reside at saturation. However, as the energetic state 2 depopulates by desorption, the molecules remaining may transform to more stable bound species. This could be a result of the weakening of adsorbate–adsorbate interactions or of the realization of different hybridization in the CO–Pt bonds. Such effects would tend to geometrically order the desorption of species 2 so that every nth molecule, for example, along a given direction on the plane would desorb before any intermediate molecule desorbs. Thus, a lattice plane partially depopulated by desorption of a single species would exhibit a periodic arrangement of empty and filled sites, in order that adsorption energy be minimized. In fact, periodic arrangements of this kind have been frequently seen in low-energy electron diffraction studies, as is described for the CO–Pt system below. It is interesting to note that the best fit identified in the above developments for the formation rate for species 2 was based on a site creation term $(n_5 + n_4)^4$. This is consistent with the postulate that species 4 and 5 are geometrically (and perhaps energetically) identical during the period of desorption of species 2.

The relation between this tendency of the adsorbed molecules to order and the mechanism governing the observed rate of formation of a particular species may be clarified by examining on the molecular scale a chemisorption of less than saturation population on a particular lattice plane. If the adsorbate is immobile at the adsorption temperature, then adsorbed molecules will begin to order only upon initiation of TPD heating. Assume for purposes of illustration that the (100) surface is populated to an extent greater than that corresponding to the sum of the saturation populations of the two most stable species, 5 and 4, but less than the total saturation population for all three species, including the least stable species 2. Rearrangement upon heating then yields a relatively complete phase characteristic of species 5 plus species 4 adsorption, with the excess mole-

cules not accommodated in this phase located at the type 2 sites thereby created. It is this latter step which determines the site dependence of the rate of formation (during TPD) for species 2, and thereby fixes the values I, J, p', and p in Eq. (6). For surface populations too small to allow completion of the ordered phase characteristic of species 5 plus species 4, it is the site dependence of species 4 which is determined by the TPD experiments in the same manner.

The last topic to be considered is the (ideal) geometric ordering of the coexisting distinct species on the various lattice plane surfaces. The ability to rationalize rate of formation dependencies and saturation populations on this basis was required of any model of the overall chemisorption. The postulated ordering of absorbed species will be illustrated for Models I and II and compared with the suggested ordering for the CO–Pt system as deduced from low-energy electron diffraction studies.

The (110) lattice plane, which has not been extensively studied by low-energy electron diffraction, is pictured at saturation population in Fig. 14. The species 7 molecules are shown adsorbed at every substrate atom lying along a "ridge" (Models I and II). If there is a second species on the (110) plane, it is postulated to be the weak species 1, which fills every other location in the "valley" (Model II). The ideal saturation population ratios are seen to be those indicated in Table 3 and are in excellent agreement with the corresponding experimental ratios. The adsorption of species 1, if it occurs, is seen to be single-site adsorption ($p = 1$), and is assumed to require the presence of the four surrounding type 7 species ($I = 7$, $p' = 4$) for creation of its site. Thus, mechanism (m) in Table 2 is rationalized.

The adsorption on the (111) plane is more complex, as shown in Fig. 15 for the saturation populations. Species 6 fills one-half the sites at saturation, and exists in either of the patterns shown. Further adsorption then occurs on the type 3 sites created by the four adjacent type 6 species, until alternate empty sites are filled (i.e., until one-quarter of the surface atoms are covered by type 3 molecules). Adsorption on the remaining one-quarter of the sites may be precluded (Model II) by the tight packing required for further adsorption [separation of 0.28 nm as compared to 0.41 nm for solid CO (4)]. If there is further adsorption, it is expected to be the weakly bound species 1, which would fill the remaining one-quarter of the sites (Model I). A c4 × 2 LEED pattern obtained for adsorption of CO on a Pt(111) single crystal was attributed to adsorption in the arrangement characterized here by the saturation population of species 6 plus species 3 (4). (See Fig. 16.) A c4 × 2 pattern has also

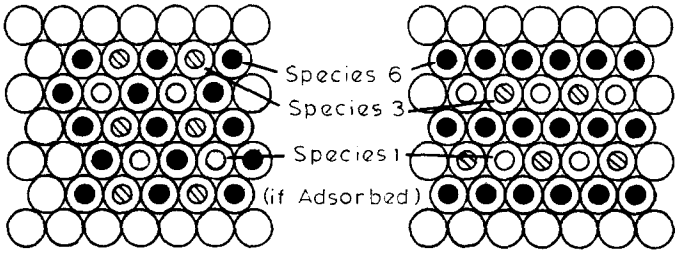

FIG. 15. Structure of the adsorbate for the (111) plane, species 6 and 3 (and 1).

been reported recently by Ertl *et al.* (*49*). Note that the absence of an adsorbed molecule at the postulated type 1 site in these LEED results does not strongly favor Model II over Model I, since the electron beam would have removed a species as weakly adsorbed as species 1. The postulated arrangement of adsorbed species is seen to correctly predict the experimental saturation population ratios of species 6 and 3. For Model I, species 1 adsorption is then considered incomplete at the arbitrarily defined "saturation" population (3600 sec at 1×10^{-8} Torr). As seen in Fig. 5, species 1 population is still increasing at 3600-sec adsorption exposure time.

In addition, rate of formation mechanisms for the (111) plane may be rationalized on the basis of the postulated arrangement of species. Species 3 adsorption is single-site adsorption ($p = 1$), requiring the presence of four adjacent type 6 species ($I = 6$, $p' = 4$) for creation of its site. This

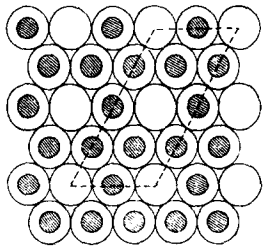

FIG. 16. The Pt–(111)–CO surface structure (*4*).

rationalizes mechanism (*g*), Table 2. In addition, if species 1 adsorbs on this plane, it is seen to be single-site adsorption ($p = 1$), requiring for the creation of its site the presence of the six now-identical adjacent species 6 and 3 ($I = 6 + 3$, $p' = 6$). The rate of formation mechanism (*k*) in Table 2 is thereby rationalized.

In fact it would be difficult to argue that at least two distinct species would not desorb from the ordered arrangement of adsorbed molecules characteristic of species 6 plus species 3. The postulated species 3

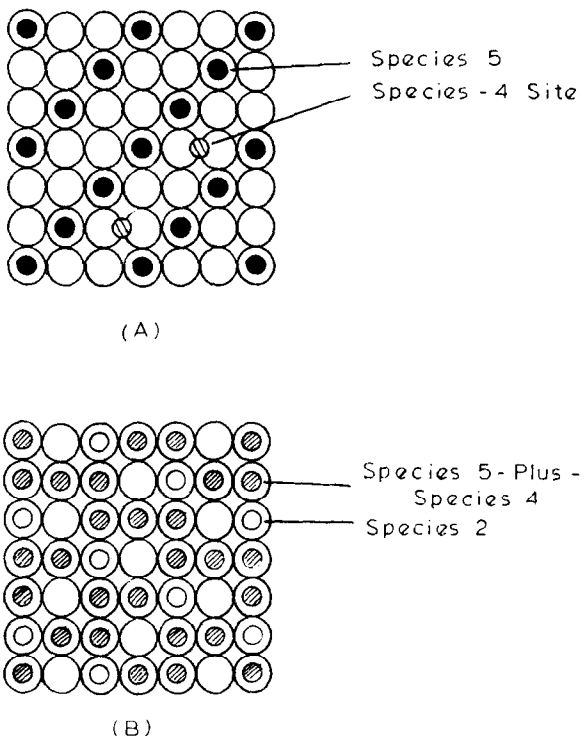

FIG. 17. Structure of the adsorbate for the (100) plane: (A) species 5 only; (B) species 5, 4, and 2.

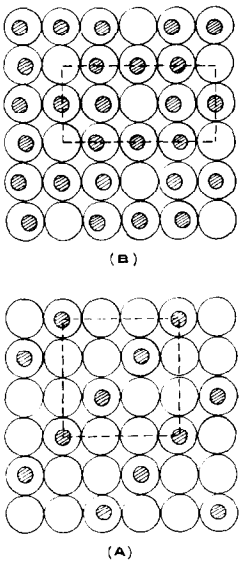

FIG. 18. (A) The Pt–(100)–($\alpha_2 + \beta$) – CO surface structure; (B) the Pt–(100)–($\alpha_1 + \alpha_2 + \beta$) – CO surface structure (*4*).

molecule desorbs from an environment of two empty and four filled adjacent sites. The postulated species 6 molecule desorbs from an environment of four to six empty adjacent sites. The question then arises as to whether a single desorption activation energy would apply in describing the desorption of all remaining type 6 molecules. With only species 6 remaining the (111) surface would be depleted to one-half or less of its saturation population. It is postulated that this density of adsorbed species would be sufficiently low to render negligible the short-range adsorbate–adsorbate interactions, thus allowing the use of a single desorption energy.

An interesting independent indication of this lack of adsorbate–adsorbate interactions arises from an analysis of the sticking probability per available site on the (111) plane, as calculated from Eq. (7). As can be seen in Fig. 13, the calculated Model I or II sticking probability per available site on the (111) plane remains approximately constant at its initial high value until species 6 has reached more than 80% of its saturation population (t_a = 200 sec). Thus, the existence on the (111) surface of both a type 3 and a type 6 adsorption state appears reasonable. It is not possible to say with certainty whether a type 1 state is present.

Finally, the chemisorption on the (100) plane is examined. That this is the most complex of the lattice plane adsorptions for this system is confirmed both in this work and in the LEED work cited here. The postulated arrangement of adsorbed molecules characteristic of type 5 adsorption at *its* saturation population is given in Fig. 17A. The coverage is one-third, and the pattern agrees with that deduced from LEED patterns for the so-called α_2 species of carbon monoxide on a Pt(100) single crystal (*4*). (See Fig. 18A.) Type 4 adsorption is postulated to be a two-site adsorption, requiring the presence of two adjacent type 5 molecules for creation of the type 4 site. The type 4 molecule might then reside at locations such as those fulfilling this description indicated in Fig. 17A. The mechanism (*d*) for the formation of species 4 is, therefore, reasonable: two-site adsorption (p = 2), depending upon the presence of two adjacent type 5 molecules (I = 5, p' = 2).

The arrangement of adsorbed molecules on the (100) surface at saturation is postulated to be that shown in Fig. 17B. The coverage is three-quarters, and again the arrangement corresponds to that deduced from LEED patterns for a complete carbon monoxide phase (α_1 plus α_2 species) on a Pt(100) single crystal (*4*). (See Fig. 18B). On the basis of the LEED patterns shown in Figs. 18A and B, a rearrangement of some adsorbed species must occur during the formation of the complete α_1 plus α_2 phase by further adsorption on a complete α_2 phase. This rearrangement is postulated to occur here upon the formation of species 2 after the species 5 plus species 4 phase is complete. A suggested location for the species 2 molecule is given in Fig. 17B. It will be noted that each empty site shown

in Fig. 17B is associated with a filled type 4 site. This and the assumed saturation coverage of three-quarters lead to the ideal population ratios given for Models I and II in Table 3. The corresponding experimental ratios are in fair agreement.

The visualization of the site dependence for the formation of species 2 according to mechanism (i) in Table 2 is difficult, since the rearrangement known to occur on the basis of the LEED patterns is thought to occur simultaneously. The species 2 molecule is bound to a single site ($p = 1$), and during formation apparently requires the presence of four adjacent identical species ($I = 5 + 4$, $p' = 4$). The species 4 and species 5 molecules are not prohibited from being identical at the saturation population density, as emphasized earlier.

In concluding the discussion, we wish to emphasize that the model deduced in this work is by no means unequivocal, but does correctly predict overall chemisorption kinetics and kinetics of formation and of desorption of individual species as determined by deconvolutions of TPD spectra. Furthermore, surface arrangements of adspecies deduced on geometric grounds from kinetic mechanisms for individual species formation are in excellent agreement with those determined in prior LEED work.

ACKNOWLEDGMENT

The authors gratefully acknowledge the financial support of the National Science Foundation.

REFERENCES

1. Good, R. H., and Müller, E. W., *Handb. Phys* **21**, 176 (1956).
2. Tucker, C. W., Jr., *J. Appl. Phys.* **35**, 1897 (1964).
3. Lyon, H. B., and Somorjai, G. A., *J. Chem. Phys.* **46**, 2539 (1967).
4. Morgan, A. E., and Somorjai, G. A., *J. Chem. Phys.* **51**, 3309 (1969).
5. Morgan, A. E., and Somorjai, G. A., *Trans. Amer. Crystallogr. Assoc.* **4**. 59 (1968).
6. Morgan, A. E., and Somorjai, G. A., *Surface Sci.* **12**, 405 (1968).
7. Smith, D. L., and Merrill, R. P., *J. Chem. Phys.* **52**, 5861 (1970).
8. Lambert, R. M., *et al.*, *Surface Sci.* **27**, 653 (1971).
9. Merrill, R. P., and Smith, D. L., *Surf. Sci.* **21**, 203 (1970).
10. Stoll, A. G., Smith, D. L., and Merrill, R. P., *J. Chem. Phys.* **54**, 163 (1971).
11. Somorjai, G. A., *Catal. Rev.* **7**, 87 (1972).
12. Clarke, T. A., Mason, R., and Tescari, M., *Surface Sci.* **40**, 1 (1973).
13. Lambert, R. M., and Comrie, C. M., *Surface Sci.* **46**, 61 (1974).
14. Kneringer, G., and Netzer, F. P., *Surface Sci.* **49**, 125 (1975).
15. Ducros, R., and Merrill, R. P., *Surface Sci.* **55**, 227 (1976).
16. Haas, T. W., Grant, J. T., and Dooley, G. J., III, *J. Vac. Sci. Technol.* **7**, 43 (1970).
17. Bonzel, H. P., and Ku, R., *Surface Sci.* **40**, 85 (1973).
18. Bonzel, H. P., and Fischer, T. E., *Surface Sci.* **51**, 213 (1975).
19. Collins, D. M., Lee, J. B., and Spicer, W. E., *Surface Sci.* **55**, 389 (1976).
20. Lewis, R., and Gomer, R., *Nuovo Cimento Suppl.* **5**, 506 (1967).
21. Eischens, R. P., Francis, S. A., and Pliskin, W. A., *J. Phys. Chem.* **60**, 194 (1956).
22. Heyne, H., and Tompkins, F. C., *Proc. Roy. Soc. Ser. A* **292**, 460 (1966).
23. Heyne, H., and Tompkins, F. C., *Trans. Faraday Soc.* **63**, 1274 (1967).
24. Seanor, D. A., and Amberg, C. H., *J. Chem. Phys.* **42**, 2967 (1965).
25. Blyholder, G., and Sheets, R., *J. Phys. Chem.* **74**, 4335 (1970).
26. Lin, K. C., Witt, J. D., and Hammaker, R. M., *Chem. Phys.* **55**, 1148 (1971).
27. Shigeishi, R. A., and King, D. A., *Surface Sci.* **58**, 379 (1976).
28. Ford, R. R., *Advan. Catal.* **21**, 51 (1970).
29. Tucker, C. W., Jr., *Surface Sci.* **2**, 516 (1964).
30. Charlot, J. M., and Deleight, R., *Compt. Rend.* **259**, 2977 (1964).
31. Burggraf, C., and Mosser, S., *Compt. Rend.* **268**, 1167 (1969).
32. Huber, W. K., and Rettinghaus, G., *J. Vac. Sci. Technol.* **7**, 289 (1970).
33. Wood, B. J., Endow, N., and Wise, H. J., *J. Catal.* **18**, 70 (1970).
34. Merrill, R. P., and Fink, S. E., *Vac. Microbalance Tech.* **8**, 55 (1971).
35. Baldwin, V. H., Jr., and Hudson, J. B., *J. Vac. Sci. Technol.* **8**, 49 (1971).
36. McCabe, R. W., and Schmidt, L. D., *Surface Sci.* **60**, 85 (1976).

37. Winterbottom, W. L., *Surface Sci.* **37**, 195 (1973).
38. Bonzel, H. P., and Ku, R., *J. Chem. Phys.* **58**, 4617 (1973).
39. Donnelly, R. G., Modell, M., and Baddour, R. F., submitted for publication.
40. Donnelly, R. G., Modell, M., and Baddour, R. F., submitted for publication.
41. Ehrlich, G., *J. Appl. Phys.* **32**, 4 (1961).
42. Redhead, P. A., *Vacuum* **12**, 203 (1962).
43. Czanderna, A. W., Biegen, J. R., and Kollen, W., *J. Colloid Interface Sci.* **34**, 406 (1970).
44. Moore, G. E., Datz, S., and Taylor, E. H., *J. Catal.* **5**, 218 (1966).
45. Data, S., Moore, G. E., and Taylor, E. H., *in* "Rarified Gas Dynamics" (J. A. Laurmann, Ed.), Vol. I, p. 347. Plenum Press, New York, 1963.
46. Kohl, W. H., "Handbook of Materials and Techniques for Vacuum Devices." Reinhold, New York, 1967.
47. Fedak, D. G., and Gjostein, N. A., *Surface Sci.* **8**, 77 (1968).
48. Mattera, A. M., Goodman, R. M., and Somorjai, G. A., *Surface Sci.* **7**, 26 (1967).
49. Ertl, G., Neumann, M., and Streit, K. M., *Surface Sci.* **64**, 393 (1977).